Author's Accepted Manuscript

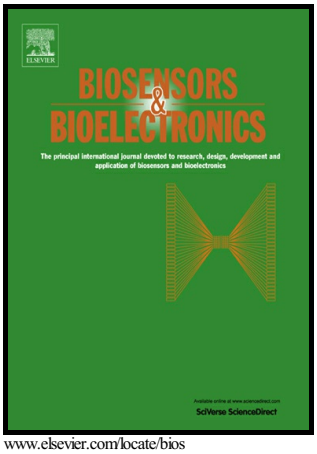

www.elsevier.com/locate/bios

A Robust, Magnetic, and Self-accelerated Electrochemiluminescent Nanosensor for Ultrasensitive Detection of Copper Ion

Yan-Mei Lei, Bai-Qi Xiao, Wen-Bin Liang, Ya-Qin Chai, Ruo Yuan, Ying Zhuo

PII: S0956-5663(18)30179-9
DOI: https://doi.org/10.1016/j.bios.2018.03.013
Reference: BIOS10339

To appear in: *Biosensors and Bioelectronic*

Received date: 1 December 2017
Revised date: 5 March 2018
Accepted date: 6 March 2018

Cite this article as: Yan-Mei Lei, Bai-Qi Xiao, Wen-Bin Liang, Ya-Qin Chai, Ruo Yuan and Ying Zhuo, A Robust, Magnetic, and Self-accelerated Electrochemiluminescent Nanosensor for Ultrasensitive Detection of Copper Ion, *Biosensors and Bioelectronic,* https://doi.org/10.1016/j.bios.2018.03.013

A Robust, Magnetic, and Self-accelerated Electrochemiluminescent Nanosensor for Ultrasensitive Detection of Copper Ion

Yan-Mei Lei, Bai-Qi Xiao, Wen-Bin Liang, Ya-Qin Chai, Ruo Yuan*,Ying Zhuo*

Key Laboratory of Luminescent and Real-Time Analytical Chemistry (Southwest University), Ministry of Education, College of Chemistry and Chemical Engineering, Southwest University, Chongqing 400715.

* Corresponding authors at: Tel.: +86 23 68252277, fax: +86 23 68253172.
E-mail addresses: yuanruo@swu.edu.cn (R. Yuan), yingzhuo@swu.edu.cn(Y.Zhuo).

ABSTRACT:

It is well known that the conventional electrochemiluminescence (ECL) biosensor rely on the heterogeneous assay formats that involves the immobilization of biorecognition probe on the electrode surface before signal collection, which inevitably cause the efficiency of bio-recognition reactions to be limited owing to the existence of local steric hindrance. Herein, a robust, magnetic, and self-accelerated ECL nanosensor based on the multifunctionalized cobalt ferrite magnetite nanoparticles ($CoFe_2O_4$ MNPs) was firstly designed for copper ion (Cu^{2+}) detection in quasi-homogeneous system. The prepared nanosensor has its unique advantages compared to the iron oxide (Fe_3O_4) MNPs-based nanosensor for which magnetic nanoparticle just provide the reaction interface and magnetic enrichment. Specifically, the prepared $CoFe_2O_4$ MNPs-based biosensing platform could bridge the gap between aqueous phase and solid materials in homogeneous solution, achieving the expansion of reaction area and the reduction of local steric hindrance with high biorecognition efficiency. Furthermore, compared with the common magnetite nanosensors, the prepared $CoFe_2O_4$ MNPs achieved a set of magnetic collection, biorecognition probes immobilization, rapid separation and signal amplification in an ECL measurement system because it could act as a new co-reaction accelerator in ECL ternary (PTC-NH_2 + $S_2O_8^{2-}$ + $CoFe_2O_4$) system, achieving a self-accelerated biosensing platform with significant enhancement of the detection sensitivity. As expected, the prepared $CoFe_2O_4$ MNPs-based ECL nanosensors were successfully applied for ultrasensitive detection of Cu^{2+} *via* click reaction with a linear range from

10^{-13} M to 1.0×10^{-7} M, which exhibited high sensitivity, excellent selectivity and good reproducibility.

Keywords: Cobalt ferrite magnetite nanoparticles, Self-accelerated, Electrochemiluminescent, Nanosensor.

1 Introduction

Electrochemiluminescence (ECL) have recently attracted considerable attention in the biosensing fields because of the promises offered by the simplified optical set-up, low background signal, and high sensitivity. (Khoshfetrat et al., 2018; Li et al., 2017; Liang et al. 2016). However, the conventional ECL biosensors rely on the heterogeneous assay formats that involves the immobilization of biorecognition probe on the electrode surface before signal collection, which are often accompanied by some intrinsic disadvantages: (1) The limited reaction area and the existence of local steric hindrance lead to relatively low binding efficiency of biorecognition probes, and thus results in low sensitivity and selectivity (Chen et al., 2017; Liu et al., 2014). (2) The fouling of the reaction interface lead to relatively poor reproducibility (Tan et al., 2015; Liu et al., 2012). Recently, magnetic nanomaterials (e.g. iron oxide magnetic nanoparticles, Fe_3O_4 MNPs) have emerged as promising bioassay nanoplatforms. For instance, Wang et al. utilized the fluorescent and colorimetric core-shell Fe_3O_4@SiO_2 NPs to build a nanosensor for Hg^{2+} detection (Wang et al., 2013). Xu's group successfully developed a smart magnetic nanosensor with PEI-coated Fe_3O_4 MNPs for cellular micoRNA detection (Wang et al., 2016). These magnetic nanoplatform could not only bridge the gap between aqueous phase and solid materials in homogeneous solution, achieving the expansion of the reaction area and reduction of the local steric hindrance with high bio-recognition efficiency, but also act as nanocarriers possessing large surface area and excellent magnetic property for the immobilization of numerous biorecognition probes and the rapid separation

from the complex matrices, providing a relatively good sensitivity, selectivity and reproducibility. However, the detection sensitivity of these nanosensors is still limited as the function of magnetic nanoparticles is just to provide the reaction interface and magnetic enrichment. Consequently, it is highly desired to develop an intelligent bioassay nanoplatform with multiple functions, which has more promising applications in ECL biosensing fields.

It is generally assumed that electrochemical reaction efficiency (ERE) is one of the most critical factors to determine the ECL intensity of luminophores. So far, the exploring of the effective coreactants is known as the most direct and simplest approach to enhance the ECL intensity as it could electrochemically react with luminophore to generate more luminophore excited state. Despite its exclusive popularity, the implementation of this approach is fundamentally restricted by drawbacks including the limited electrochemical reactivity and the limited types of effective coreactant. To overcome these problems, recently, our group have found another effective approach, namely, the co-reaction accelerator amplification strategy to improve the ERE of luminophore and coreactant by introduction another reagent in the binary system, where the co-reactant accelerator could interact with coreactant to generate more reactive intermediates or transition states to improve the ERE of luminophore and coreactant. For example, some amine compounds and nanomaterials could act as the co-reactant accelerator to construct the novel ECL ternary system, such as semicarbazide in the CdTe quantum dots/$S_2O_8^{2-}$ system (Ma et al., 2015) and TiO_2 nanoflowers in the silver nanoclusters/dissolved O_2 system

(Zhou et al., 2017). Herein, a new kind of coreaction accelerator of multifunctionalized cobalt ferrite magnetite nanoparticles ($CoFe_2O_4$ MNPs) was introduced in amino-terminated perylene derivative (PTC-NH_2)/$S_2O_8^{2-}$ system, where the $CoFe_2O_4$ MNPs could not only use as a nanocarrier with large surface area and excellent magnetic property, but also could act as a new co-reaction accelerator, achieving a self-accelerated biosensing platform with significant enhancement of ERE of PTC-NH_2 and $S_2O_8^{2-}$.

Copper ion (Cu^{2+}) is a micronutrient required for several necessary processes in the human body, while its excess has been largely disclosed to be directly correlated with cancer progression, tumor burden, incidence, regression and reoccurrence (Wang et al., 2017; Zhang et al., 2017). In this work, a robust, magnetic, and self-accelerated ECL nanosensor based on the multifunctionalized $CoFe_2O_4$ MNPs was firstly developed for the first time, and then for highly sensitive and selective detection of target Cu^{2+} *via* click reaction in quasi-homogeneous system. Specifically, the terminal azido-functionalized thiol strands (DNA1) were immobilized on the surface of Au nanoparticles-modified $CoFe_2O_4$ MNPs to acquire ECL nanosensor. In presence of target Cu^{2+}, the initiator strands of terminal alkynyl (DNA2) were linked to DNA1 strands with the help of ascorbic acid (AA, which could reduce Cu^{2+} to Cu^{+}) based on Cu^{+}-catalyzed click chemistry reaction (Xie et al., 2016; Shen et al., 2014). Subsequently, the initiator strands of DNA1 were expected to trigger hybridization chain reaction (HCR), resulting in the generation of a long-nicked dsDNA molecule. Then, the ECL signal tags of PTC-NH_2 were intercalated into the dsDNA grooves *via*

electrostatic adsorption, intermolecular hydrophobic and π-π stacking interactions (Hu et al., 2017; Wang et al., 2016). Finally, the prepared $CoFe_2O_4$ MNPs-based nanosensors were detected in $S_2O_8^{2-}$ solution under the external magnetic field to achieve a significantly amplified ECL signal. As a result, on the basis of the changes of the ECL intensities which were correlated to the concentrations of target Cu^{2+}, the $CoFe_2O_4$ MNPs-based ECL nanosensors were successfully applied for ultrasensitive detection of Cu^{2+} with high sensitivity, excellent selectivity and good reproducibility.

2 Experiment

2.1 Preparation of $CoFe_2O_4$ magnetic nanoparticles

The $CoFe_2O_4$ magnetic nanoparticles (MNPs) were synthesized by a one-pot hydrothermal method according to the published literature with a minor modification as follows (Deng et al., 2005). $FeCl_3$•$6H_2O$ (0.54 g, 2 mM) and $Co(NO_3)_2$•$6H_2O$ (0.29 g, 1 mM) were dissolved in 16 mL of ethylene glycol to form a clear solution, followed by the addition of 1.44 g NaAc, 1.2 g urea and 0.4 g polyethylene glycol. Thereafter, the mixture was stirred vigorously for 45 min, and then the reddish brown mixture was transferred into a Teflon-lined stainless-steel autoclave with 20 mL capacity, heated to 200 ^oC for 10 h and finally cooled to room temperature. The black products were collected under the magnetic field, washed alternately with ultrapure water and ethanol, and dried at 60 ^oC for 5 h.

2.2 Fabrication of $CoFe_2O_4$ MNPs-based ECL nanosensors

The preparation of $CoFe_2O_4$ MNPs-based ECL nanosensors involved four steps. The first step was to decorate the dopamine (DA) on the $CoFe_2O_4$ MNPs surface according to the literature (Ye et al., 2015) with slight modifications. Typically, 5 mg $CoFe_2O_4$ MNPs were dispersed in a mixture containing 2.0 mL THF solution and 2.0 mL dopamine (DA) aqueous solution (1%, w/w) under constant ultrasonification for 1 h. Then 2.0 mM acetic acid solution was introduced to adjust the pH value of the mixed solution to 4.0. The obtained solution was continued to shake for 12 h, during which DA molecules could make the surface of $CoFe_2O_4$ MNPs hydrophilic and positively-charged. After that, the DA modified $CoFe_2O_4$ MNPs was washed with ultrapure water three times under the magnetic field, and then redispersed in 2.0 mL ultrapure water. As a second step, 8.0 mL colloidal gold nanoparticles (Au NPs) solution was added to the resultant DA modified $CoFe_2O_4$ MNPs solution, followed by gentle shaking for 15 h, during which the negatively charged Au NPs could be electrostatically attracted onto the surface of DA modified $CoFe_2O_4$ MNPs. Subsequently, the Au NPs modified $CoFe_2O_4$ MNPs (Au@$CoFe_2O_4$ MNPs) was washed with ultrapure water three times under the magnetic field, and then redispersed in 5.0 mL Tris-HCl buffer. In the third step, 500 μL DNA1 (100 μM, terminal azido-functionalized thiol) solution was added to the resultant Au@$CoFe_2O_4$ MNPs solution, followed by gentle shaking for 24 h at 4 ^oC. After that, the Au@$CoFe_2O_4$ MNPs/DNA1 was washed with Tris-HCl buffer solution three times under the magnetic field, and then redispersed in 5.0 mL Tris-HCl buffer. In the four step, 1.0 mL HT (1 mM) solution was added into the resultant Au@$CoFe_2O_4$ MNPs/DNA1 solution with shaking for 2 h at 4 ^oC to block the nonspecific binding sites. The purified $CoFe_2O_4$ MNPs-based ECL nanosensors (Au@$CoFe_2O_4$/DNA1/HT) were obtained by magnetic separation, and then

redispersed in 10.0 mL Tris-HCl buffer at 4 ^{o}C for further use. And Scheme 1A summarized the fabrication process of the $CoFe_2O_4$ MNPs-based ECL nanosensors.

2.3 Copper ion (Cu^{2+}) assay of $CoFe_2O_4$ MNPs-based nanosensors

First, 20 μL of different concentrations of Cu^{2+} solution, 5 μL AA solution (10 mM) and 50 μL DNA2 solution (5 μM) was successively added to 500 μL $CoFe_2O_4$ MNPs-based ECL nanosensors solution, followed by gently shaking for 2 h at room temperature. In this process, the initiator strands of DNA2 were linked to DNA1 strands with the help of Cu^{2+} and ascorbic acid *via* click chemistry. Subsequently, 100 μL hairpin probe H1 (5 μM) and 100 μL hairpin probe H2 (5 μM) was added in the resultant $CoFe_2O_4$@Au/DNA1/HT/DNA2 solution and then continued to shake for 2 h, during which the DNA2 were expected to trigger hybridization chain reaction (HCR) to achieve a long-nicked dsDNA molecule. Following that, 100 μL PTC-NH_2 solution (5 mg mL^{-1}, synthesized as shown in Supporting Information 1.3) was added in the resultant $CoFe_2O_4$@Au/DNA1/HT/DNA2/dsDNA solution and then continued to shake for 2 h at room temperature, during which the ECL signal tags of PTC-NH_2 were intercalated into the dsDNA grooves *via* electrostatic adsorption, intermolecular hydrophobic and π-π stacking interactions. After each step the corresponding products were collected under the magnetic field and washed with Tris-HCl buffer to remove the physically absorbed species. Finally, the prepared magnetic products was added into 3 mL of 10 mM $K_2S_2O_8$ (pH 7.4) solution, and then detected with a homemade three-electrode system under the magnetic field (prior to each experiment, the gold circular plate was cleaned as shown in Supporting Information 1.4). The working potential was from -2.0 to 0 V (*vs*. Ag/AgCl) with a scan rate of 0.3 V/s and the voltage of the photomultiplier tube (PMT) was set at 800 V in the detection

process. Scheme 1B and 1C summarized the reaction and measurement process of the prepared $CoFe_2O_4$ MNPs-based ECL nanosensors, respectively.

Scheme 1

3. Results and discussion

3.1 Characterization of different nanomaterials

As shown in Fig. 1A, the typical HRTEM images of $CoFe_2O_4$ MNPs exhibited a spherical shape with a diameter of 40±20 nm (which was smaller than the ~200 nm diameter $CoFe_2O_4$ MNPs reported in the literature (Deng et al., 2005), indicating that these $CoFe_2O_4$ MNPs could provide high surface areas and allow for the immobilization of numerous biorecognition probes. In addition, the $CoFe_2O_4$ MNPs dispersed compactly, which could be attributed to the magnetic dipole-dipole attractions (Lalatonne et al., 2004). Then the HRTEM images of Au@$CoFe_2O_4$ MNPs was shown in Fig. 1B. The diameter of the Au@$CoFe_2O_4$ MNPs was not obviously changed compared with that of $CoFe_2O_4$ MNPs, but it was interesting to observe that plentiful dark nanoparticles were coated on the core surface of $CoFe_2O_4$ MNPs. Meanwhile, the spheres distribution changed from compactness to sparseness, which might be that the surface of $CoFe_2O_4$ MNPs was coated by the hydrophilic DA molecules *via* complexation (Xie et al., 2010). From the enlarged HRTEM image of Au@$CoFe_2O_4$ MNPs (Fig. 1C), it could be clearly found that the Au NPs with the size 5.0±2 nm were distributed on the surface of $CoFe_2O_4$ MNPs. In addition, the EDS spectrum of the Au@$CoFe_2O_4$ MNPs showed the peaks of Co, Fe, O, and Au elements (Fig. 1 D), which clearly hinted towards the presence of Au NPs on the

surface of the $CoFe_2O_4$ MNPs.

Fig. 1

The UV-Vis absorption spectrum of the dopamine modified $CoFe_2O_4$ MNPs and Au@$CoFe_2O_4$ MNPs were shown in Fig. 2A. A new maximum absorption peak of Au@$CoFe_2O_4$ MNPs was located at ~535 nm (curve *a*) in comparison with that of the dopamine modified $CoFe_2O_4$ MNPs (curve *b*), indicating that the successful decoration of Au NPs on the surface of the dopamine modified $CoFe_2O_4$ MNPs (Zhao et al., 2013). The room-temperature magnetization curves of the dopamine modified $CoFe_2O_4$ MNPs and Au@$CoFe_2O_4$ MNPs were depicted in Fig. 2B. The saturation magnetization of the dopamine modified $CoFe_2O_4$ MNPs and Au@$CoFe_2O_4$ MNPs are 56.78 emu g^{-1} (curve *a*) and 52.49 emu g^{-1} (curve *b*), respectively. The little decrease in magnetization for Au@$CoFe_2O_4$ MNPs could be attributed to the diamagnetic contribution of Au NPs coated outside (Salgueiriño-Maceira et al., 2006). However, the Au@$CoFe_2O_4$ MNPs still showed strong magnetization, which suggested their suitability for magnetic separation.

Raman spectroscopy demonstrated that ECL signal tags of PTC-NH_2 was successfully intercalated into the dsDNA grooves. As shown in Fig. 2C, the $CoFe_2O_4$ MNPs-based nanosensors were implement the homogeneous reaction process (as shown in Scheme 1B) except the incubation of PTC-NH_2 solution, which exhibited the strongest peak at ~1490 cm^{-1} (curve *a*). However, when the prepared $CoFe_2O_4$ MNPs-based nanosensors incubated with PTC-NH_2 solution, six characteristic peaks between 1050 and 1710 cm^{-1} could be observed in curve *b*. These results

demonstrated that the PTC-NH_2 as ECL signal tags were intercalated into the dsDNA grooves (Brown et al., 2012).[24] In addition, as shown in Fig. 2D, the prepared $CoFe_2O_4$ MNPs-based nanosensors incubated with PTC-NH_2 solution could be separated easily and quickly under external magnetic field (part a), which demonstrated that the feasibility of the prepared $CoFe_2O_4$ MNPs-based nanosensors for target assay in complex matrix solution. Furthermore, the prepared $CoFe_2O_4$ MNPs-based nanosensors incubated with PTC-NH_2 solution in both neutral (pH 7.4) and alkaline (pH 12.0) environments was separated under UV-visible irradiation, respectively (Fig. 2D, part b). It could be found the fluorescence of PTC-NH_2 molecules was quenched under neutral conditions, owing to the aggregation of PTC-NH_2 molecules in the dsDNA (Wang et al., 2011; Hu et al., 2015).[25,26] However, the positive charge density of the ECL signal tags (PTC-NH_2) was decreased in basic conditions, which made the PTC-NH_2 release from the dsDNA grooves, and thereby appeared yellow fluorescence. It was further demonstrated that the PTC-NH_2 as ECL signal tag was intercalated into the dsDNA grooves.

Fig. 2.

3.2 The possible ECL mechanism of ternary (PTC-NH_2 + $S_2O_8^{2-}$ + $CoFe_2O_4$) system

To verify the ECL mechanism of ternary (PTC-NH_2 + $S_2O_8^{2-}$ + $CoFe_2O_4$) system, ECL responses and CV curves of the different ECL systems were collected synchronously by using the homemade three-electrode system, and these results were illustrated in Fig. 3. It could be observed a cathodic ECL peak about 328 a.u in $S_2O_8^{2-}$ solution (Fig. 3A, curve *a*), which was corresponding to the emission of the singlet

oxygen ($^1(O_2)_2^*$) (Niu et al., 2011). And the corresponding CV wave showed an obvious reduction peak at -1.14 V (Fig. 3B, curve *a*), which could be assigned to the reduction of $S_2O_8^{2-}$ (Fabrizio et al., 2000). Subsequently, an evident increase of the ECL response was observed in PTC-NH_2 + $S_2O_8^{2-}$ solution (about 3195 a.u; Fig. 3A, curve *b*), which could be ascribed to the fact that the co-reactant $S_2O_8^{2-}$ could react with the luminophore PTC-NH_2 to produce the excited state of PTC-NH_2 and thus exhibited a strong ECL response. And the corresponding CV wave displayed an apparently reduction peak where the reduction potential shifted positively from -1.14 V to -0.48 V and the peak current increased apparently (Fig. 3B, curve *b*), which could be assigned to the strong oxygenation between PTC-NH_2 and $S_2O_8^{2-}$ (Ma et al., 2015). Afterwards, a slightly enhanced ECL signal about 521 a.u was observed in $CoFe_2O_4$ + $S_2O_8^{2-}$ solution (Fig. 3A, curve *c*) in comparison with that of $S_2O_8^{2-}$ solution (Fig. 3A, curve *a*), indicating that the $CoFe_2O_4$ could promote the reduction of $S_2O_8^{2-}$ to generate more $SO_4^{-\bullet}$, and thus emit strong light. Meanwhile, the corresponding peak current value was noticeably increased (Fig. 3B, curve *c*) in comparison with that of $S_2O_8^{2-}$ solution (Fig. 3B, curve *a*), which could be ascribed to the increasing concentration of H^+ on the electrode surface in $S_2O_8^{2-}$ solution (Ma et al., 2015). Remarkably, when $CoFe_2O_4$ MNPs was introduced in ECL binary (PTC-NH_2 + $S_2O_8^{2-}$) system, the ECL peak intensity was noticeably increased from 3195 a.u (Fig. 3A, curve *b*) to 9869 a.u (Fig. 3A, curve *d*). Therefore, we speculated that $CoFe_2O_4$ could be acted as a co-reaction accelerator in ECL ternary (PTC-NH_2 + $S_2O_8^{2-}$ + $CoFe_2O_4$) system. Specifically, the co-reaction accelerator ($CoFe_2O_4$) could interact with coreactant ($S_2O_8^{2-}$) rather than luminophore (PTC-NH_2) to generate more $SO_4^{\bullet-}$, and thus promote the ECL reaction efficiency of PTC-NH_2 + $S_2O_8^{2-}$

system, resulting in producing more of the excited state of PTC-NH_2 to emit stronger light. And the corresponding CV wave showed an obvious reduction peak at -0.88 V (Fig. 3B, curve *d*) and the peak current increased distinctly in comparison with that of PTC-NH_2 + $S_2O_8^{2-}$ solution (Fig, 3B, curve *b*), which might be that the $CoFe_2O_4$ could promote the reduction of $S_2O_8^{2-}$ to generate more $SO_4^{-\bullet}$, and thereby enhance the interaction between PTC-NH_2 and $S_2O_8^{2-}$. Furthermore, when $CoFe_2O_4$ was introduced in PTC-NH_2 solution, predictably, a weak ECL signal was observed in same potential range (Fig. 3A, curve *d*), further demonstrating that the $CoFe_2O_4$ could not interact with the PTC-NH_2 to amplify the ECL signal. And the corresponding CV wave exhibited two pairs of redox peaks, which could be ascribed to the multielectron transfer of PTC-NH_2 (Lei et al., 2015). That is to say, the co-reaction accelerator of $CoFe_2O_4$ was introduced in ECL ternary (PTC-NH_2 + $S_2O_8^{2-}$ + $CoFe_2O_4$) system, which could interact with coreactant ($S_2O_8^{2-}$) rather than luminophore (PTC-NH_2) to produce more $SO_4^{-\bullet}$, and thus enhance ERE of PTC-NH_2 and $S_2O_8^{2-}$ to emit stronger ECL signal.

Fig. 3.

As shown in Fig. 4A, the normalized ECL spectrum were also collected to further identify the ECL mechanism of PTC-NH_2 + $S_2O_8^{2-}$ + $CoFe_2O_4$ system. The ECL spectrum of $S_2O_8^{2-}$ solution with the maximum emission wavelength at 575 nm (Fig. 4A, curve *a*) was consistent with the emission of $CoFe_2O_4$ + $S_2O_8^{2-}$ system (Fig. 4A, curve *b*), which could be ascribed to the emission of $^1(O_2)_2^*$ (Yao et al., 2008). Meanwhile, the ECL spectrum of PTC-NH_2 + $S_2O_8^{2-}$ + $CoFe_2O_4$ system with a maximum at 675 nm (Fig. 4A, curve *b*) was consistent with the emission of the PTC-NH_2 + $S_2O_8^{2-}$ system, which could be assigned to the emission of the excited

PTC-NH_2 (π-excimers, $^1(PTC\text{-}NH_2)_2^*$) (Lei et al., 2015). It was further demonstrated that the luminophore was the $^1(PTC\text{-}NH_2)_2^*$ and the $CoFe_2O_4$ acted as a new co-reaction accelerator in ternary (PTC-NH_2 + $S_2O_8^{2-}$ + $CoFe_2O_4$) system. And the possible ECL mechanism of the binary (PTC-NH_2 + $S_2O_8^{2-}$) system and the ternary (PTC-NH_2 + $S_2O_8^{2-}$ + $CoFe_2O_4$) system could be illustrated as Fig. 4B and 4C, respectively.

Fig. 4

3.3 The performance of $CoFe_2O_4$ MNPs-based nanosensors

The calibration curve for Cu^{2+} detection. The ECL measurements were used to quantitatively assess the prepared $CoFe_2O_4$ MNPs-based nanosensors for the determination of Cu^{2+} according to the protocol described in experimental section. As depicted in Fig. 5A, the ECL intensity gradually increased with the increased Cu^{2+} concentrations (curve *a* to *g*), indicating that the Cu^{2+} concentration was quantitatively measured by the ECL peak signal. The calibration plot for the quantitative detection of Cu^{2+} was illustrated in Fig. 5B. The ECL intensity (I) was linearly proportional to the logarithm of the Cu^{2+} concentration in the range from 1.0 × 10^{-13} M to 1.0×10^{-7} M. As a result, a linear regression equation was I = 1407.57 lg c + 125749.50 (where I represents ECL intensity and c represents Cu^{2+} concentration) with a correlation coefficient of R = 0.9986 and a detection limit of 3.3×10^{-14} M (S/N = 3). In addition, as shown in Table 1, the prepared $CoFe_2O_4$ MNPs-based nanosensors were compared with other assays for Cu^{2+} detection (as shown in the Supporting Information 1.7). These results showed that the prepared $CoFe_2O_4$

MNPs-based nanosensors provided an more effective way as well as a wider dynamic concentration response range for Cu^{2+} detection.

Fig. 5

Selectivity and stability of the prepared $CoFe_2O_4$ MNPs-based nanosensors. The stability of the prepared $CoFe_2O_4$ MNPs-based nanosensors were evaluated under consecutive cyclic potential scans for 16 cycles during the cyclic potential scanning between -2.0 and 0 V. As shown in Fig. 5C, the ECL intensity did not show any obvious changes with relative standard deviations (RSD) of 1.62 %, indicating that the outstanding stability of the prepared $CoFe_2O_4$ MNPs-based nanosensors. As shown in Fig. 5D, the selectivity of the prepared $CoFe_2O_4$ MNPs-based nanosensors were also evaluated by against other interference metal ions (Zn^{2+}, Fe^{2+}, Ni^{2+}, Ca^{2+}, Cd^{2+}, Pb^{2+}, Hg^{2+}, Mg^{2+} and Co^{2+}) at a concentration of 1.0×10^{-7} M and target Cu^{2+} at 1.0×10^{-10} M. Compared to that of the blank target Cu^{2+}, no remarkable ECL changes were observed, indicating that the prepared $CoFe_2O_4$ MNPs-based nanosensors displayed good selectivity for target Cu^{2+} detection.

3.4 Direct detection of Cu^{2+} in human hair solutions

We had performed an experiment to evaluate the accuracy of the prepared $CoFe_2O_4$ MNPs-based ECL nanosensors. As shown in as shown in the Supporting Information 1.8 (Table. S3), the concentrations of Cu^{2+} in human hair extracted solution (the human hair sample pretreatment process as shown in the Supporting Information 1.9) were determined by the $CoFe_2O_4$ MNPs-based nanosensors as well

as inductively coupled plasma mass spectrometric (ICP-MS) method. According to the statistic calculation by a t test (a = 0.1), the concentrations of the $CoFe_2O_4$ MNPs-based nanosensors displayed fairly good concordance compared with ICP-MS method (t = 0.74, which are smaller than the standard t value of 2.13), indicating that this $CoFe_2O_4$ MNPs-based nanosensors had a capacity for determining Cu^{2+} in practical sample analysis.

4 Conclusions

In conclusion, we devised a robust, magnetic, and self-accelerated ECL nanosensor based on the multifunctionalized $CoFe_2O_4$ MNPs for the trace Cu^{2+} detection. Such a device was different from the conventional heterogeneous ECL assay formats for which the heterogeneous assay was subject to the relatively low biorecognition efficiencies as well as poor reproducibility. The multifunctionalized $CoFe_2O_4$ MNPs used here could not only act as nanocarriers with the expansion of the reaction area, reduction of the local steric hindrance and feasibility of magnetic separation and enrichment, allowing for immobilization of numerous biorecognition probes and the rapid separation from the complex matrices, but also act as a new co-reaction accelerator in ECL ternary (PTC-NH_2 + $S_2O_8^{2-}$ + $CoFe_2O_4$) system, achieving a strong ECL signal. As a result, these $CoFe_2O_4$ MNPs-based ECL nanosensors showed high sensitivity, excellent selectivity and good reproducibility for Cu^{2+} detection *via* click reaction in quasi-homogeneous system, which held great promise as a useful tool for reliable and sensitive detection of other analytes.

Acknowledges

This work was financially supported by the NNSF of China (21675130, 21575116, 21675129, 21775124), and the Fundamental Research Funds for the Central Universities **(**XDJK2016E056), China.

Appendix A. Supplementary material

Supplementary data associated with this article can be found in the online version at doi:

References

Brown, K.E., Veldkamp, B.S., Co, D.T., Wasielewski, M.R. 2012. J. Phys. Chem. Lett. 3, 2362-2366.

Chen, S., Chen, X., Zhang, L., Gao, J., Ma, Q. 2017. ACS Appl. Mater. Interfaces 9, 5430-5436.

Deng, H., Li, X., Peng, Q., Wang, X., Chen, J., Li, Y. 2005. Angew. Chem., Int. Ed. 117, 2842-2845.

Fabrizio, E.F., Prieto, I., Bard, A.J. 2000. J. Am. Chem. Soc. 122, 4996-4997.

Hu, R., Zhang, X., Xu, Q., Lu, D. Q., Yang, Y. H., Xu, Q. Q., Ruan, Q., Mo, L.T., Zhang, X. B. 2017. Biosens. Bioelectron. 92, 40-46.

Hu, Z., Chen, J., Li, W., Wang, Y., Li, Y., Sang, L., Li, J., Zhang, Q., Ibupoto, Z., Yu, C. 2015. Anal. Chim. Acta. 895, 89-94.

Khoshfetrat S.M, Bagheri H, Mehrgardi M.A. 2018. Biosens. Bioelectron. 100, 382-388.

Lalatonne, Y., Richardi, J., Pileni, M.P. 2004. Nature Mater. 3, 121-125.

Lei, Y.M., Huang, W.X., Zhao, M., Chai, Y.Q., Yuan, R., Zhuo, Y. 2015. Anal. Chem. 87, 7787-7794.

Li, N.L., Jia, L.P., Ma, R.N., Jia, W.L., Lu, Y.Y., Shi, S.S., Wang, H.S. 2017. Biosens. Bioelectron. 89, 453-460.

Liang, W.B., Yang, M.Z., Zhuo, Y., Zheng, Y.N., Xiong, C.Y., Chai, Y.Q., Yuan, R. 2016. Chem. Sci. 7, 7094-7100.

Liu, M., Zhao, H., Chen, S., Yu, H., Quan, X. 2012. Environ. Sci. Technol. 46, 12567-12574.

Liu, S., Lin, Y., Wang, L., Liu, T, Cheng, C., Wei, W., Tang, B. 2014. Anal. Chem. 86, 4008-4015.

Ma, M.N., Zhuo, Y., Yuan, R., Chai, Y.Q. 2015. Anal. Chem. 87, 11389-11397.

Niu, H., Yuan, R., Chai, Y.Q., Mao, L., Yuan, Y., Zhuo, Y., Yuan, S., Yang, X. 2011. Biosens. Bioelectron. 26, 3175-3180.

Salgueiriño-Maceira, V., Correa-Duarte, M.A., Spasova, M., Liz-Marzán, L.M., Farle, M. 2006. AdV. Funct. Mater. 16, 509-514.

Shen, Q.P., Zhou, L.F., Yuan, Y.J., Huang, Y., Xiang, B.B., Chen, C.Y., Nie, Z., Yao, S.Z. 2014. Biosens. Bioelectron. 55, 187-194.

Tan, Y., Wei, X., Zhao, M., Qiu, B., Guo, L., Lin, Z., Yang, H.H. 2015. Anal. Chem. 87, 9204-9208.

Wang, B., Jiao, H., Li, W., Liao, D., Wang, F., Yu, C. 2011. Chem. Commun. 47, 10269-10271.

Wang, B., Wu, Y., Chen, Y., Weng, B., Xu, L., Li, C. 2016. Biosens. Bioelectron. 81, 125-130.

Wang, J., Li, R.S., Zhang, H.Z., Wang, N., Zhang, Z., Huang, C.Z. 2017. Biosens. Bioelectron. 97, 157-163

Wang, M., Hou, X., Wiraja, C., Sun, L., Xu, Z.J., Xu, C. 2016. ACS Appl. Mater. Interfaces 8, 5877-5886.

Wang, W., Zhang, Y., Yang, Q.B., Sun, M.D., Fei, X.L., Song, Y., Zhang, Y.M., Li, Y.X. 2013. Nanoscale 5, 4958-4965.

Xie, H.Y., Zhen, R., Wang, B., Feng, Y.J., Chen, P., Hao, J. 2010. J. Phys. Chem. C 114, 4825-4830.

Xie, Q., Weng, X., Lu, L., Lin, Z., Xu, X., Fu, C. 2016. Biosens. Bioelectron. 77, 46-50.

Yao, W.; Wang, L.; Wang, H.Y.; Zhang, X.L. 2008. Electrochim. Acta 54, 733-737.

Ye, M., Wei, Z., Hu, F., Wang, J., Ge, G., Hu, Z., Shao, M., Lee,S.T., Liu, J. 2015. Nanoscale 7, 13427-13437.

Zhang, H., Feng, L., Jiang, Y., Wong, Y.T., He, Y., Zheng, G., He, J., Tan, Y., Sun, H., Ho, D. 2017. Biosens. Bioelectron. 94, 24-29.

Zhao, Y., Zhang, W., Lin, Y., Du, D. 2013. Nanoscale 5, 1121-1126.

Zhou, Y., Wang, H.J., Zhuo, Y., Chai, Y.Q.,Yuan, R. 2017. Anal. Chem. 89, 3732-3738.

Figure Captions

Scheme 1. Schematic illustration of the $CoFe_2O_4$ MNPs-based ECL nanosensors assay: (A) the fabrication process of the $CoFe_2O_4$ MNPs-based ECL nanosensors, (B) the homogeneous reaction process of the prepared nanosensors for target Cu^{2+} detection, and (C) the enriched solid-state ECL measurement process of the prepared nanosensors in 3.0 mL of 10 mM $S_2O_8^{2-}$ solution (pH 7.4). The cross-sectional view (D) and image (E) of homemade three-electrode system.

Fig. 1. Typical HRTEM images of (A) $CoFe_2O_4$ MNPs and (B) Au@$CoFe_2O_4$ MNPs, (C) the enlarged HRTEM image of Au@$CoFe_2O_4$ MNPs. (D) EDS spectrum of the Au@$CoFe_2O_4$ MNPs.

Fig. 2. (A) UV-vis absorption spectrum and (B) Room-temperature magnetization curves: (a) the dopamine modified $CoFe_2O_4$ MNPs and (b) Au@$CoFe_2O_4$ MNPs. (C) Raman spectrum: the $CoFe_2O_4$ MNPs-based nanosensors implemented the homogeneous reaction process (as shown in Scheme 1B) after incubated (a) without and (b) with PTC-NH_2 solution. (D) Photographic images: the $CoFe_2O_4$ MNPs-based nanosensors implemented the homogeneous reaction process (as shown in Scheme 1B) after incubated with PTC-NH_2 solution in an external magnetic field (a) without and (b) with UV-visible irradiation.

Fig. 3. ECL responses (A) and CV curves (B) were collected synchronously by using the homemade three-electrode system (scan range: -2.0 to 0 V, *vs* Ag/AgCl; scan rate, 0.3 V/s): (a) $S_2O_8^{2-}$ solution, (b) PTC-NH_2 + $S_2O_8^{2-}$ solution, (c) $CoFe_2O_4$ + $S_2O_8^{2-}$ solution, (d) PTC-NH_2 + $S_2O_8^{2-}$ + $CoFe_2O_4$ solution and (e) PTC-NH_2 + $CoFe_2O_4$ solution. The concentration of PTC-NH_2, $S_2O_8^{2-}$, and $CoFe_2O_4$ were 1 mg/mL, 10 mM, and 2 mg/mL in PBS solution (0.1 M, pH 7.4), respectively.

Fig. 4. (A) Normalized ECL spectrum of (a) $S_2O_8^{2-}$ solution, (b) $CoFe_2O_4$ + $S_2O_8^{2-}$ solution, (c) PTC-NH_2 + $S_2O_8^{2-}$ + $CoFe_2O_4$ solution, and (d) PTC-NH_2 + $S_2O_8^{2-}$ solution, respectively. The possible ECL mechanism for (B) the PTC-NH_2 + $S_2O_8^{2-}$ system and (C) PTC-NH_2 + $S_2O_8^{2-}$ + $CoFe_2O_4$ system, respectively.

Fig. 5. (A) ECL profiles of the prepared $CoFe_2O_4$ MNPs-based nanosensors after

incubated with Cu^{2+} at various concentrations: 10^{-13}, 10^{-12}, 10^{-11}, 10^{-10}, 10^{-9}, 10^{-8}, 10^{-7} M (from *a* to *g*) based on the proposed detection principle. (B) The calibration plot of the ECL intensity versus the logarithm of Cu^{2+} concentration. (C) ECL stability of the prepared $CoFe_2O_4$ MNPs-based nanosensors under consecutive cyclic potential scans (Cu^{2+} concentration at 1.0×10^{-11} M). (D) Selectivity of the prepared $CoFe_2O_4$ MNPs-based nanosensors toward Cu^{2+} (1.0×10^{-7} M) by comparing it to the interfering metal ions (1.0×10^{-10} M).

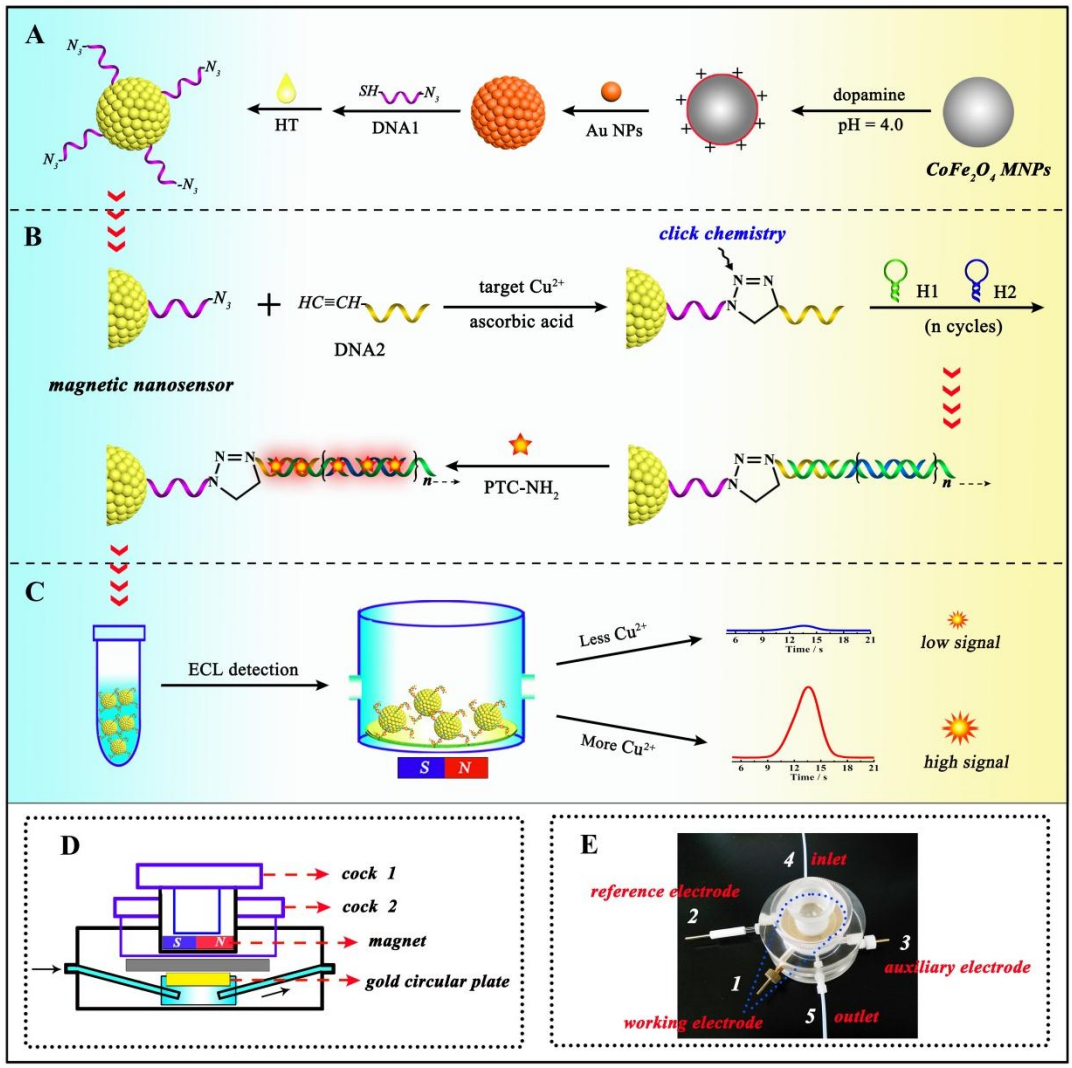

Scheme 1. Schematic illustration of the $CoFe_2O_4$ MNPs-based ECL nanosensors assay: (A) the fabrication process of the $CoFe_2O_4$ MNPs-based ECL nanosensors, (B) the homogeneous reaction process of the prepared nanosensors for target Cu^{2+} detection, and (C) the enriched solid-state ECL measurement process of the prepared nanosensors in 3.0 mL of 10 mM $S_2O_8^{2-}$ solution (pH 7.4). The cross-sectional view (D) and image (E) of homemade three-electrode system.

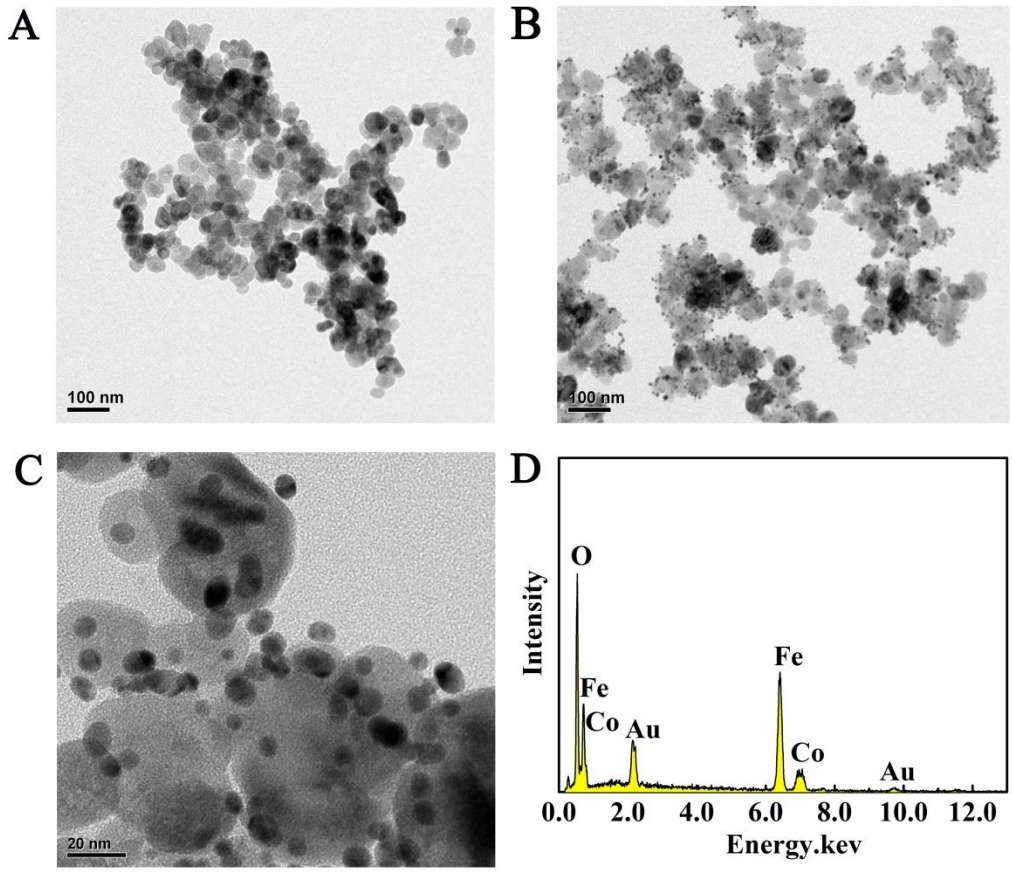

Fig. 1. Typical HRTEM images of (A) $CoFe_2O_4$ MNPs and (B) Au@$CoFe_2O_4$ MNPs, (C) the enlarged HRTEM image of Au@$CoFe_2O_4$ MNPs. (D) EDS spectrum of the Au@$CoFe_2O_4$ MNPs.

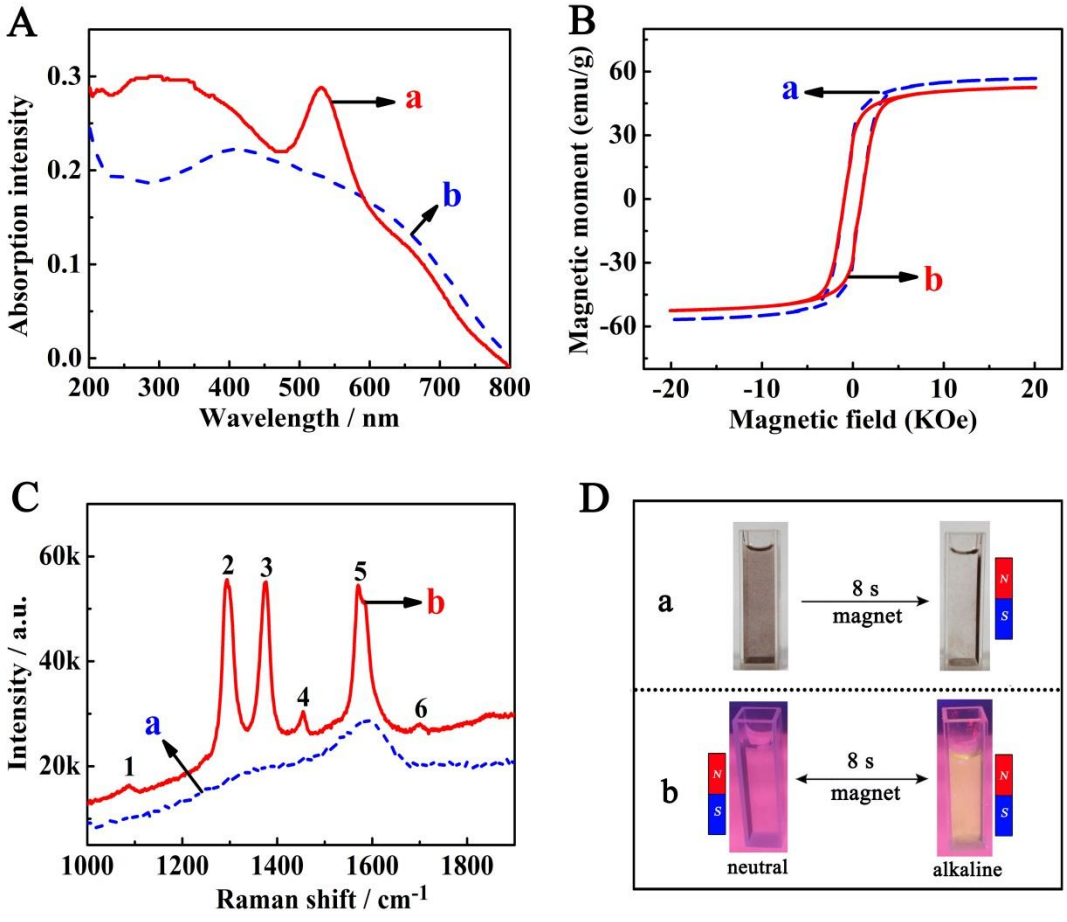

Fig. 2. (A) UV-vis absorption spectrum and (B) Room-temperature magnetization curves: (a) the dopamine modified $CoFe_2O_4$ MNPs and (b) Au@$CoFe_2O_4$ MNPs. (C) Raman spectrum: the $CoFe_2O_4$ MNPs-based nanosensors implemented the homogeneous reaction process (as shown in Scheme 1B) after incubated (a) without and (b) with PTC-NH_2 solution. (D) Photographic images: the $CoFe_2O_4$ MNPs-based nanosensors implemented the homogeneous reaction process (as shown in Scheme 1B) after incubated with PTC-NH_2 solution in an external magnetic field (a) without and (b) with UV-visible irradiation.

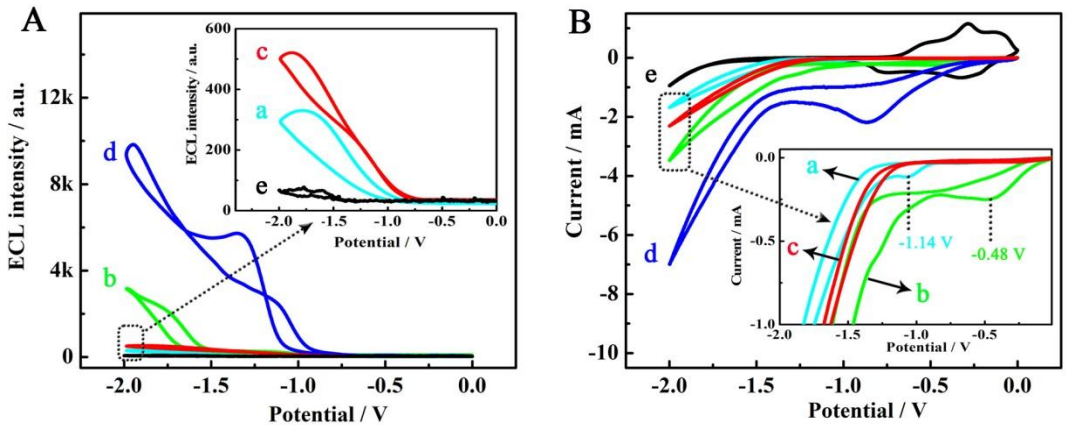

Fig. 3. ECL responses (A) and CV curves (B) were collected synchronously by using the homemade three-electrode system (scan range: -2.0 to 0 V, *vs* Ag/AgCl; scan rate, 0.3 V/s): (a) $S_2O_8^{2-}$ solution, (b) PTC-NH_2 + $S_2O_8^{2-}$ solution, (c) $CoFe_2O_4$ + $S_2O_8^{2-}$ solution, (d) PTC-NH_2 + $S_2O_8^{2-}$ + $CoFe_2O_4$ solution and (e) PTC-NH_2 + $CoFe_2O_4$ solution. The concentration of PTC-NH_2, $S_2O_8^{2-}$, and $CoFe_2O_4$ were 1 mg/mL, 10 mM, and 2 mg/mL in PBS solution (0.1 M, pH 7.4), respectively.

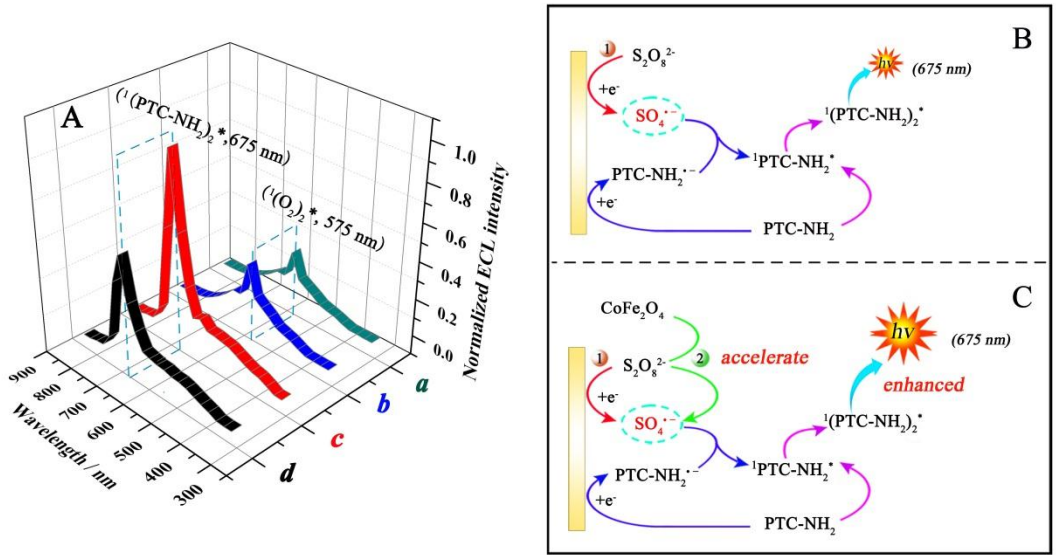

Fig. 4. (A) Normalized ECL spectrum of (a) $S_2O_8^{2-}$ solution, (b) $CoFe_2O_4$ + $S_2O_8^{2-}$ solution, (c) PTC-NH_2 + $S_2O_8^{2-}$ + $CoFe_2O_4$ solution, and (d) PTC-NH_2 + $S_2O_8^{2-}$ solution, respectively. The possible ECL mechanism for (B) the PTC-NH_2 + $S_2O_8^{2-}$ system and (C) PTC-NH_2 + $S_2O_8^{2-}$ + $CoFe_2O_4$ system, respectively.

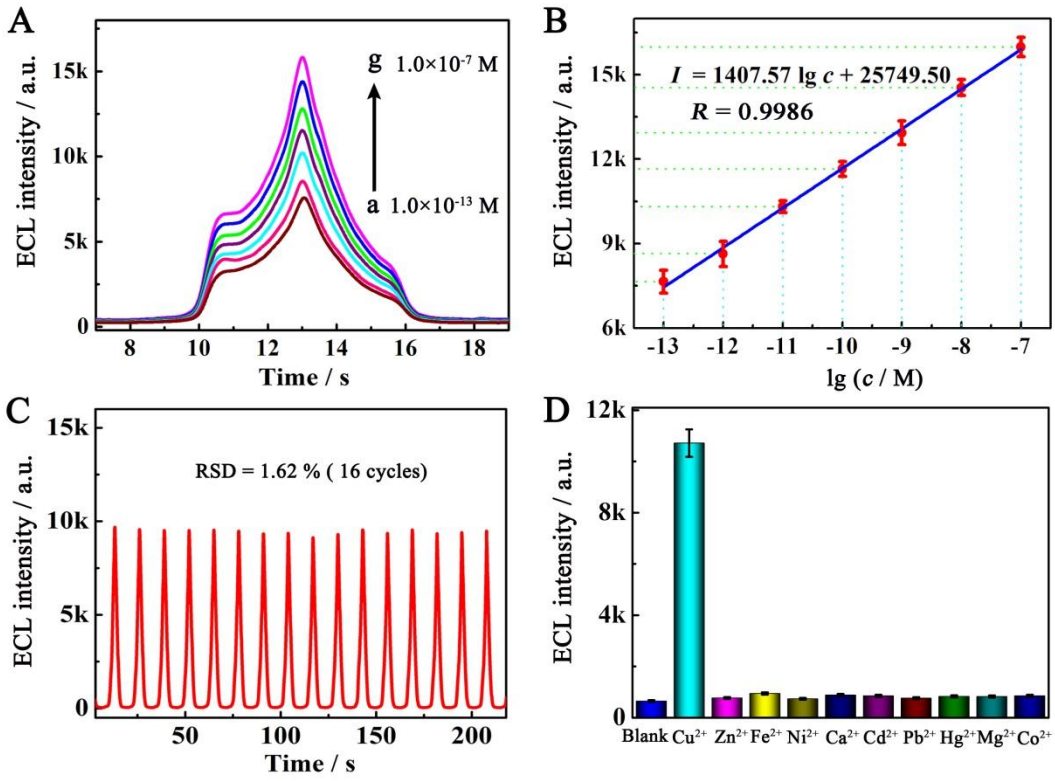

Fig. 5. (A) ECL profiles of the prepared $CoFe_2O_4$ MNPs-based nanosensors after incubated with Cu^{2+} at various concentrations: 10^{-13}, 10^{-12}, 10^{-11}, 10^{-10}, 10^{-9}, 10^{-8}, 10^{-7} M (from *a* to *g*) based on the proposed detection principle. (B) The calibration plot of the ECL intensity versus the logarithm of Cu^{2+} concentration. (C) ECL stability of the prepared $CoFe_2O_4$ MNPs-based nanosensors under consecutive cyclic potential scans (Cu^{2+} concentration at 1.0×10^{-11} M). (D) Selectivity of the prepared $CoFe_2O_4$ MNPs-based nanosensors toward Cu^{2+} (1.0×10^{-7} M) by comparing it to the interfering metal ions (1.0×10^{-10} M).

For TOC only:

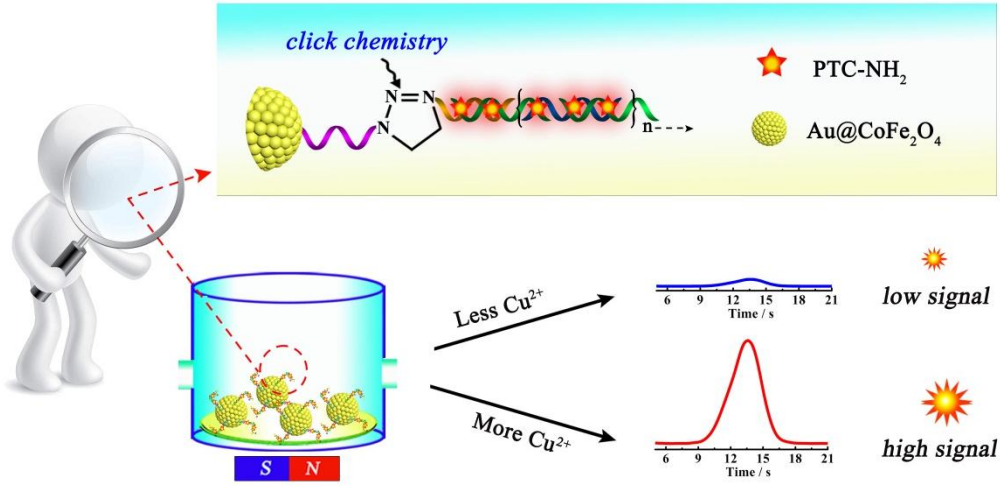

High lights

- The $CoFe_2O_4$ MNPs was used to develop an intelligent bioassay nanoplatform with multiple functions.
- The $CoFe_2O_4$ MNPs could act as co-reaction accelerator in ECL ternary system to enhance ECL signal.
- The **nanosensor** achieved a sensitive detection of Cu^{2+} in quasi-homogeneous system.